# MATHEMATIC MODELLING, SIMULATION, TEST AND CORRELATION OF A CAPTURE BEFORE CONTACT DOCKING MECHANISM

**Alejandro Lázaro [(1)], Javier Viñals [(1)]**

*[(1)] SENER Aeroespacial, Avd. Zugazarte, 56, 48930 Getxo, Bizkaia (Spain), Email:alejandro.lazaro@aeroespacial.sener*

## ABSTRACT

This paper focuses on the mathematic modelling, simulations, and testing of SENER's multifunctional interface, SIROM, as a berthing/docking mechanism for space vehicles. SIROM aims to move towards a more flexible and smarter interface suitable for heterogeneous space missions. The paper provides an overview of the main features of SIROM, including its androgynous design, high-capture range latches, self-aligning capability, and compact design. Additionally, the paper discusses the integration of proximity sensor switches for docking purposes and presents a geometrical study on the capture range and a simulation analysis of SIROM's docking capabilities. The results show the feasibility of SIROM as a docking interface and provide insights into possible design enhancements.

## 1 INTRODUCTION

In the frame of current European space projects, multi-functional interfaces (I/F) emerge as a cornerstone to facilitate standardization of future's connection among space vehicles. However, the functional needs of these interfaces are expected to evolve along with future space mission's requirements. In this context, SENER's multifunctional interface –SIROM [1]– seeks to move towards a more flexible and smarter interface, suitable for a wide variety of missions by offering a solution able to perform docking operations.

In this paper, the mathematic modelling, simulations, and testing of SIROM as a berthing/docking mechanism for space vehicles is presented. On the one hand, it aims at shedding light on SIROM's suitability as docking/berthing I/F; and, on the other hand, detect possible design enhancements.

## 2 CONTEXT

SIROM (Standard Interconnect for Robotic Manipulation), as its name evinces, was born as a Standard Interconnect (SI) during the first call of PERASPERA project (2016-2019) [1] [2]. I/Fs of this kind are focused on the transfer functionalities between vehicles/ORUs, for either data, power, thermal or fluid transfer. SI can have multiple interconnection applications: spacecraft-to-spacecraft, payload-to-payload, payload-to-spacecraft, tool changer, etc.

By default, SIs are neither intended to act as main rigid contact point between spacecrafts nor perform first contact during docking operations. Nevertheless, SIROM presents promising mechanical features – such as latches that enable capture without contact, and alignment petals – rising the possibility of usage for docking scenarios.

The recent participation of SENER in Projects founded by the European Commission –EROSS-IOD, ORUBOAS and PoC-01 [3]– has offered a broad perspective on the needs of future space logistic ecosystems, resulting into a new generation of SIROM families with the ultimate goal of offering a flexible and configurable module for those future missions –see Figure 1–.

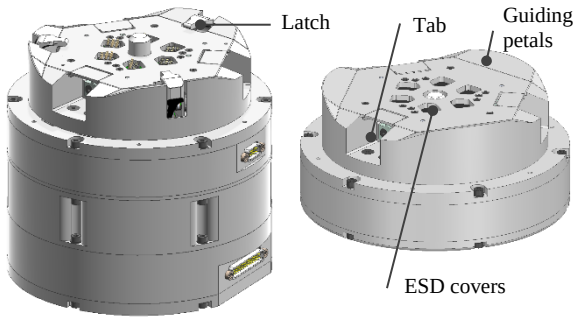


*Figure 1.*Left: Active SIROM E. Right: Passive SIROM E. New generation units for data and power transfer

## 3 MECHANISM DESCRIPTION

Main features of SIROM mechanism are:

- Androgynous design: Active versions capable of capture either a Passive or an identical configuration.
- Cost optimized: Passive version designed to reduce costs when multiple matting ports are needed to be installed.
- The latches of the Active SIROM are responsible of capturing (before contact) the Passive SIROM and establish the required preload to clamp the assembly.
- High-capture range latches based on docking system for ISS. The mechanism includes three capture hooks (or latches) evenly distributed 120º apart.
- Self-aligning capability after contact using guiding petals.
- Compact design including data, electrical and fluid transfer capabilities. Mass <1,5kg.

- High-pressure fluid connector with minimal leakage.
- Deployable covers to protect the electronic components from electro-static discharge (ESD).
- Motor-based actuation to preform 3 operations: mechanical capture, covers deployment and connectors matting.

## 4 PROXIMITY SENSOR SWITCH FOR DOCKING PURPOSES

As main addition to ease docking, the next generation SIROMs integrate a hall-effect sensors-based capture switch. This system enables the mechanical capture once the capturing I/F is within the capture envelope of the I/F to be captured.

The selection of a magnet and hall sensor pair is constrained by the mechanical capabilities of SIROM. Therefore, the logical procedure starts from the comprehension of the I/F's capture possibilities and ends up with switch definition. Currently, different alternatives are being studied, considering 2 or 3 hall effect sensors. The variables over which there are room to play are: sensors detection threshold, magnets sizing and relative position.

It must be highlighted the importance to tune/adjust to coincide both parts, to prevent premature or late latch closures which could result into undesired re-bounces or deterioration of the latches themselves. Moreover, the aforementioned tuning is challenging since the magnetic flux surrounding magnets do not have a uniform spatial distribution –see Eq.1 Eq.2 [4] and Figure 2–.

$$B_\rho = \frac{\mu_o \mu}{4\pi} \frac{3\rho z}{r^5} \quad (1)$$

$$B_z = \frac{\mu_o \mu}{4\pi} \frac{(2z^2 - \rho^2)}{r^5} \quad (2)$$

Where:

- $B$: magnetic field (T)
- $\mu$: magnetic permeability ($N \cdot A^{-2}$)
- $\rho$: radial coordinate (m)
- $z$: vertical coordinate (m)
- $r$: magnet radius (m)

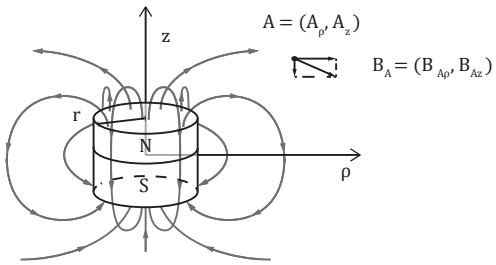


*Figure* 2.- *Magnetic flux created by cylindrical magnet.*

## 5 CAPTURE RANGE GEOMETRICAL STUDY

As for an initial procedure to analyse correct capture positions, geometrical modelling for different static spatial positions is formulated. Each latch is represented as a point that must fall within a box representing the opposing unit's capture's envelope –named as tab–, as shown in Figure 3. Thereby, for different relative positions three latches' position with respect to their corresponding tab are assessed, concluding whether the capture is correct or unsuccessful.

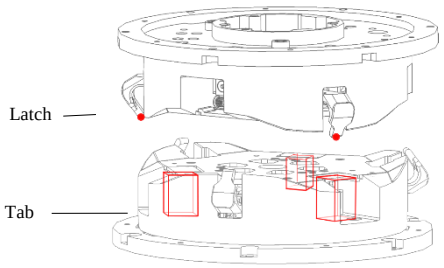


*Figure 3.* SIROM latch and tab representation for the mathematical modelling.

A campaign following a discrete distribution is conducted within a selected plane to assess the effect of rotational misalignment in the behaviour prior to contact.

As it can be observed in Figure 4, for a perfect relative alignment scenario the capture range is of the order of ±6mm on the plane, forming a dodecagon. Conversely, as the misalignment in three axis raises –roll, pitch, yaw– the dodecagon shape turns into a smaller triangle. Lastly, for a rotation of 6º in yaw, the fully contactless capture allows values of the order of ±2mm on the plane.

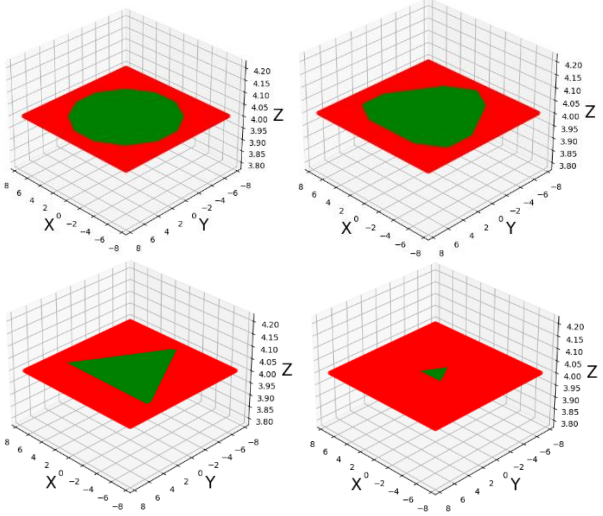


*Figure 4. Top Left: captures in green with RPY = 0º. Top Right: captures in green with RPY=1º. Bottom Left: captures in green with RPY = 3º. Bottom Right: captures in green with RP=0º and Y=6º.*

The last graph is intended to visualize the higher impact on the capture envelope of deviations on the yaw axis

than rotation on the pitch and roll axes. As positive remark, current GNC visual navigation-based systems reach an attitude control on the yaw more accurate than on the roll and yaw, reaching deviations lower than 1 degree. Considering large deviations on the yaw axis are not likely to happen, the capture range previous to contact will remain close to ±6mm.

Therefore, disregarding the effect before contact, the capture envelope describes a dodecagon when SIROMs perfectly aligned. This geometry results from the intersection of 3 rectangular prism rotation of 120º respect their yaw axis. Likewise, the increase of the relative angle between I/Fs results in considerably smaller capture envelopes, tending to triangular shapes due to SIROMs triangular symmetry.

Pointing out the main limitation of this approach, it represents the problem as static disregarding the effect of residual velocities experienced in rendezvous operations. Although GNC rendezvous systems positional accuracy is moving towards the order of millimetres, fixed relative positioning is still hardly achievable. Therefore, this mathematical representation includes uncertainty when it comes to determine how valid a position close to the boundaries of the capture envelope is in reality. As shown in Figure 5, there might be trajectories that could hinder the capture, even detecting the hall sensor at certain moment. Note that these trajectories are represented as straight lines, disregarding navigation errors, and the capture operation will require to be aborted by means of additional rendezvous sensors.

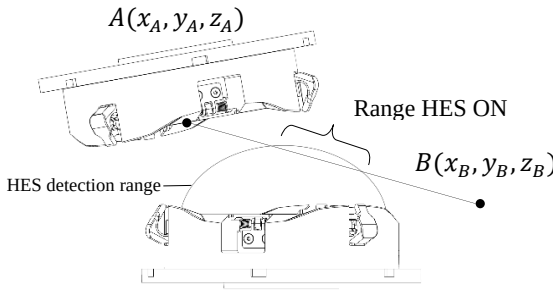


*Figure 5. Trajectory resulting in incorrect captures.*

Likewise, as a second limitation, the response after contact is not assessed, which means that just a small fraction of the behaviour when docking can be comprehended by means of this approach.

## 6 DOCKING CAPABILITIES SIMULATION

This section describes the procedure followed to analyse SIROM interfaces' capability to perform docking operations. It complements the previous section study by offering insights on the behaviour after contact.

In this context, a dynamic trajectories simulation model is set up using ADAMS software. This model considers the displacement of a SIROM unit from a point A –a singular point in the space– to B –located within the capture envelope of a second SIROM– actuating the latching mechanism once a certain distance from the target B is reached. This distance is meant to represent the hall effect-based trigger; nonetheless, it does not fully mimic the real performance. It derives from the simplification of the trigger's activation zone, which relies on the interaction of the magnetic flux produced by the magnets with the hall-effect sensors.

The docking simulator includes 2 SIROM units fixed to servicer and client vehicles in free floating conditions –6 DoFs–. These vehicles can be customized to analyse the effect of changes on the mass, CoG position and inertia. Additionally, by means of a rotational damping tool in ADAMS the behaviour of reaction wheels can be emulated on the desired vehicles. Figure 6 illustrates the general structure of the model. For this study, two identical vehicles of 250kg and 1x1x1 $m^3$ envelope without reaction wheels are selected.

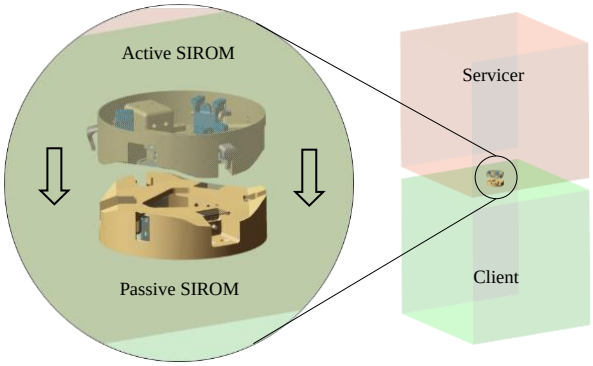


*Figure 6.- Docking simulator scheme in ADAMS.*

The analysis consists of a combinatoric campaign where certain variables presented in Table 1 adopt values within the specified range – $x_1$, $y_1$–. The decision of lowering the rotational alignment range with respect to the mathematical model –reached up to 6º in yaw and 3º combined– derives from the interaction with SENER's GNC department.

*Table 1. Variables controlled in the simulation.*

| Controlled variable | Range |
|---|---|
| Initial position | $x_0$:0m, $y_0$: 0m, $z_0$: 0.04m |
| Final position | $x_1$, $y_1$ range ±0.020m $z_1$: 0m |
| Rotational alignment | Pitch, roll, yaw: 0º or 1º |
| Sequence time | 8s |
| Capture start distance | 0.01m |

Table 2 includes the *velocity* and *hall effect-based trigger* activation instant which are dependent on the *Sequence time* and *Capture start distance*, respectively.

*Table 2. Variables indirectly controlled.*

| Indirectly controlled | Equation and range |
|---|---|
| Velocity | $\frac{\sqrt{(x_0-x_1)^2+(y_0-y_1)^2+(z_0)^2}}{t}$ (3) <br> $0.005\text{m/s} < \text{v} < 0.007\text{m/s}$ |
| Hall effect-based trigger | $\frac{t\left(\sqrt{(x_0-x_1)^2+(y_0-y_1)^2+(z_0)^2}-l_{hall}\right)}{\sqrt{(x_0-x_1)^2+(y_0-y_1)^2+(z_0)^2}}$ (4) <br> $0.7\text{s} < \text{t} < 1\text{s}$ |

A 21 x 21 point's grid varying the final positioning on the plane $-x_1$ and $y_1$ variables– is studied, resulting in 441 simulations per each orientation –from Eq.5– .

$$V_2^{21} = 21^2 = 441 \quad (5)$$

After running the analysis, results are plotted in Figure 7. It makes use of the following colour code to represent different observed responses:

- Green: correct capture cases.
- Red: cases where capture does not occur, resulting in rebounds.
- Yellow: captured with 2 out of 3 latches.
- Orange: the allowable impact or torque supplied by the motors is exeeded.
- The space lefts blank represent cases where simulation fails.

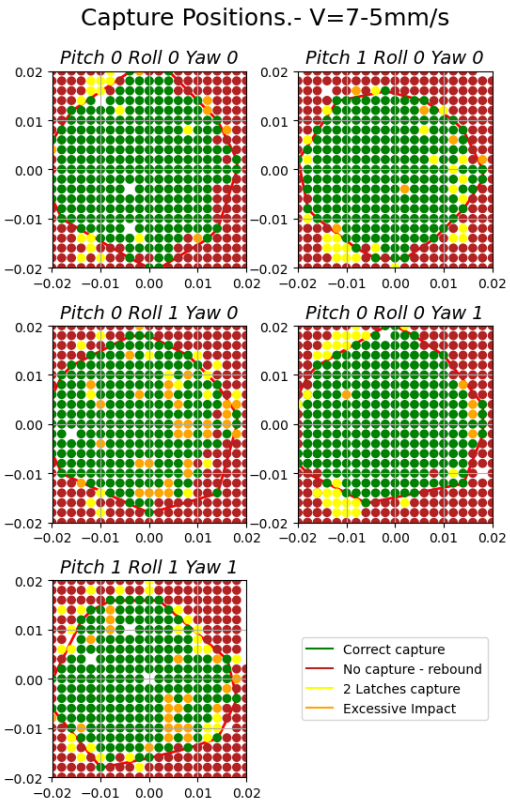


*Figure 7.- Capture envelope for 250kg servicer and client configuration.*

Lastly, a comparison between simulations in ADAMS and the mathematical modelling is performed. Note that the mathematical model is limited to the analysis of static positions, whereas the simulation in ADAMS represents a dynamic behaviour. Known the context, it is decided to compare the results obtained in ADAMS with the instant where the latch it intermediately deployed axially. The maximum deployment is shown in Figure 8.

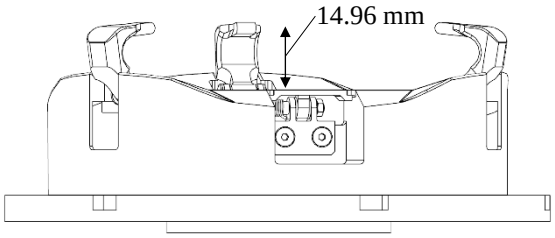


*Figure 8.- Latch fully deployed and axial tolerance to capture.*

From prior knowledge, it is known that the latch adopts its maximum deployment at 15% of its aperture travel. Considering in ADAMS the capture is configured to start at a 9mm of the target I/F –see Table 1–, at 7.65mm the fully deployed position is obtained. This value is close to the middle of the tolerance –14.96mm– to maximize the captures when misaligned. Thus, in the mathematical model static positions at 7.65 mm are assessed. Table 3 includes the comparison between simulated and mathematical models.

*Table 3. Capture comparison between ADAMS and mathematical models -C: Capture. NC: No Capture-*

| ADAMS | MATH | COUNT | PERCENTAGE |
|---|---|---|---|
| C | C | 215 | 9.6 % |
| C | NC | 971 | 43.2 % |
| NC | C | 8 | 0.4 % |
| NC | NC | 1056 | 46.9 % |

The mathematical model considers that out of the 2250 cases only 223 (215+8) captures, whereas the simulation 1186 (971+215). This evinces the box and dots representations of the mathematical model is over restrictive. However, the current mathematical model's false positive rate is 0.4%, which makes it highly reliable. In other words, if a capture is mathematically possible, it is highly likely to be certain in the simulation.

Lastly, as it was anticipated with the mathematical model in Figure 4, Figure 7 reassures the effect of the increase of misalignment reshaping capture envelope towards a triangle.

As main outcome, the tests conducted on the kinematic model evinces different results for a same trajectory when approach velocity, relative mases and inertias vary.

## 7 CAPTURE SWITCH

This section presents the mathematical modelling and implementation of a hall effect sensor –HES– based system to effectively trigger the correct timing for capture command. This system intends to provide SIROM with an integrated and reliable solution to detect whether a capture is possible or not. It contemplates to integrate 2 or 3 HES sensors. The approach followed starts by adding features to the geometrical model presented in Section 5 and ends up with a test in robotic setup for correlation purposes.

### 7.1 Geometrical study

The capture geometrical model presented in Section 5 is enhanced by including the HESs and magnets positioning in accordance with their disposition within SIROM units.

As for the implementation on the model, first the flux around the magnet is obtained for discrete points. These values are used as source for a three-dimensional interpolation to compute the specific flux of a position of a HES. Lastly, this flux value is compared with the detection threshold of the HES, obtaining the state -on or off-.

Regarding the definition of the geometrical model, a dataset is constructed by following a discrete distribution with 6 variables –x, y, z, pitch, roll, yaw–. This dataset is intended to be used not only for the computational analysis, but also testing on the robotic setup. The aforementioned variables are studied within the ranges shown in Table 4.

*Table 4. Geometrical model variables' range*

| Variable | Min | Max |
|---|---|---|
| x | -4 mm | 4 mm |
| y | -4 mm | 4 mm |
| z | 3.67 mm | 11 mm |
| roll | -6.3º | 6.3º |
| pitch | -6.3º | 6.3º |
| yaw | -6.3º | 6.3º |

Some cases are ruled out because they represent an incongruous positioning where a SIROM penetrates in its counterpart unit. The full dataset consist of 4352 cases after eliminating the incongruous cases.

In this case, 3 magnets of 4mm of both diameter and height is used and 3 HES with a sensibility of 2.5mT is considered. From the analysis the correct capture cases are obtained and plotted in Figure 9.

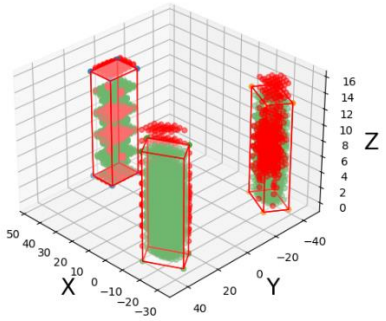


*Figure 9.- Captures. Tabs and Latches representation.*

Table 5 includes the correlation between capture and HES status and the objective of each combination. It must be stated that HES system's false positives are considered critical, jeopardizing docking operation's success.

*Table 5. Results of 3Hall/Capture Simulations*

| HES | CAP | COUNT | % | OBJECTIVE |
|---|---|---|---|---|
| ON | C | 1591 | 36.56% | Maximize |
| ON | NC | 0 | 0.00% | Minimize |
| OFF | C | 2320 | 53.31% | Reduce |
| OFF | NC | 441 | 10.13% | Maximize |

From the cases computed it can be observed that the current HES-based trigger guarantees a correct performance, where 0% of the cases are considered critical. However, in 53.31% out of the total cases the trigger is invalidating the capture, even though this last being possible. Therefore, either increasing the magnet size or HES's tolerance seems a logical step to move forward as long as the false positive rate stays low – close to current 0% –.

Table 6 presents the results for a trigger composed of 2 HES.

*Table 6. Results of 2Hall/Capture Simulations*

| HES | CAP | COUNT | % | OBJECTIVE |
|---|---|---|---|---|
| ON | C | 1543 | 35.45% | Maximize |
| ON | NC | 6 | 0.14% | Minimize |
| OFF | C | 2368 | 54.41% | Reduce |
| OFF | NC | 435 | 10.00% | Maximize |

As it can be observed the performance obtained by both models are considerably similar. However, including 2 HES results in the impossibility of perceiving the rotations respect to the axis formed by the 2 HEDs. In addition, the false positive rate increases up to 0.14%, which makes 2 HES-based system less desirable. Therefore, from the geometrical study evidence on the preferability of including 3 HES is obtained.

### 7.2 Implementation

The robotic setup consist of a U10 robot [6] mounting a SIROM as end-effector, and a second SIROM unit mounted on a fixed position on the workbench. –See Figure 10– Commercial hall-effect sensors with a threshold value of 2.5mT and magnets with 4mm of both diameter and height are included in both units.

The robot follows an operational sequence starting from a I/Fs' relative position of 10cm in the z axis towards the desired position. When the desired position is reached the HES state is recorded.

The target point coincides with the 4352 cases used for the geometrical study. These are translated from an axis-angle representation –rotation vector– to a three basic vectors configuration –rotation matrix– by means of Rodrigues rotation formula [5]. The rationale behind this decision comes from the operational baseline of a U10 robot [6] –which uses rotation vector– and the intent to replicate the simulated positions.

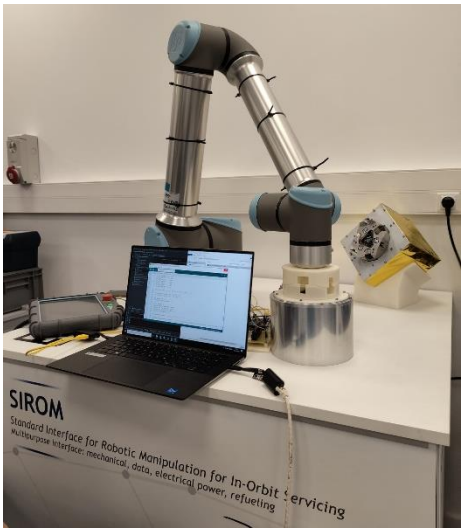


*Figure 10.- Robotic setup*

The test is conducted for the same 2250 cases mentioned in Section 7.1 and is repeated in three occasions, for the following cases:

- **Test 1** with 2 HES.
- **Test 2** with 2 HES right after the first round to assess the repeatability.
- **Test 3** with 3 HES to assess the effect on the performance of an additional sensor.

*Table 7. Correlation between **Hall simulations** and **Hall tests** in the robotic setup*

| | TEST 1 | TEST 2 | TEST 3 |
|---|---|---|---|
| Correlation success rate | 70.40% | 69.49% | 56.25% |

*Table 8. Correlation between **Capture simulations** and **Hall tests** in the robotic setup*

| HES | CAP | TEST 1 | TEST 2 | TEST 3 |
|---|---|---|---|---|
| ON | C | 42.07% | 41.77% | 34.54% |
| ON | NC | 0.51% | 0.48% | 0.53% |
| OFF | C | 47.79% | 48.09% | 55.35% |
| OFF | NC | 9.63% | 9.65% | 9.58% |

Test 1 and test 2 account for the same setup, and the obtained similarity rate is 89.40%.

Looking at the results illustrated in Table 7, including an additional HES reduces the success rate, since it implies the activation of an additional sensors in a system that is not optimal at this point.

Likewise, from the physical testing is observed that having 2 HESs in one interface brings up a risk regarding the impossibility to capture the rotation with respect to the axis formed by the 2 HESs. Despite this risks, 2 HES's system result in a better performance than 3 HES's system.

In addition, Table 8 confirms the HES system being suboptimal, presenting a detection range considerably small, restricting the capture possibilities.

## 8 CONCLUSIONS

This section is divided in two parts: capture envelope and capture switch, gathering relevant outcomes on the performed study with the intent to tune SIROM to maximize its capture possibilities.

### 8.1 Capture envelope

The mathematical model enables a fast iterative process, limited to assess what happens due to I/F's contact. In this context, the kinematic model emerges as a complementary approach to the mathematical modelling, to get initial insights on the performance of SIROM in free floating scenarios after docking.

Likewise, the original capture envelope of SIROM (+-5mm in the plane) it is likely to be extended after running the pertinent tests. This conclusion is extremely promising, considering the flexibility that increasing the capture range till 10mm would provide to the GNC side.

### 8.2 Capture switch

The closed-loop mathematical model emerges as a tool to iterate on HES and magnet selection, and positioning within the I/F. It provides a fast iterative tool to get initial insights on the performance to be further complemented with physical tests on the robotic system.

The poor correlation between simulated and tested HES does still entail certain complexity, however several hypotheses that could cause this phenomenon are considered. a) The sensibility threshold of HES could be below the specified by the supplier. b) The magnets and halls positioning in 3D printed mock-ups present wide tolerances, which could result in total deviances of the order of millimetre. c) Robotic setup presents some backlash at starting motion, which could displace the SIROM mounted on the table.

The tests on the robotic setup seem to require a more restrictive control of the tolerances, adjustments, coordinate system's definition.

## 9 NEXT STEPS

The obtained results reveal an inefficient reduction of the capture possibilities to increase the reliability of the HES detection system. In fact, even though the current kinematic model presents a capture range of the order of centimetres, for the HES system detection range is correlated with the mathematical results, being this last of the order of millimetres. Thus:

$$Kinematic\ envelope > Math.envelope > HES\ range$$

Therefore, it might be promising to either increase the magnet size or find a HES with higher sensitivity. In case none of these improvements allow the capture switch to obtain an accurate performance, alternative detection technologies will be explored. Moreover, the difficulty to comprehend the realism of simulated contacts might require correlating the model with real testing. Therefore, testing in air-bearing or robotic facilities is proposed to simulate 3DoF or 6DoF floating conditions, respectively and to correlate results derived from the kinematic model.

Lastly, the inclusion of residual rotational speeds and flexible contacts between SIROM and vehicle are targeted as improvements to be included in the kinematic simulator.

## 10 ACKNOWLEDGEMENT

The authors would like to thank all the supporting staff and partners who contributed to the development of SIROM.

SENER is actively involved in the following projects founded by the European Commission improving and seeking the adoption of SIROM as standard interface:

- EROSS-IOD under grant agreement Nº 101082464.
- ORU-BOAS under grant agreement Nº 101082078.

## 11 REFERENCES

[1] V. Javier *et al.*, 'Systems and Infrastructures to Implement Future Building Blocks in Space Exploration and Development - multi-functional interface for payload interconnection of robotic systems in space', presented at the IAC-18-D3.2, 69th International Astronautical Congress, Bremen, Germany, Oct. 2018.

[2] 'Periodic Reporting for period 1 - SIROM (Standard Interface for Robotic Manipulation of Payloads in Future Space Missions) | H2020 | CORDIS | European Commission'. https://cordis.europa.eu/project/id/730035/reporting (accessed May 30, 2023).

[3] G. Shelikhov, 'Building the European Space Logistics Ecosystem for In-Space Transportation', *ESA Commercialisation Gateway*, Sep. 02, 2022. https://commercialisation.esa.int/2022/09/building-the-european-space-logistics-ecosystem-for-in-space-transportation-2/ (accessed May 30, 2023).

[4] N. Derby and S. Olbert, 'Cylindrical magnets and ideal solenoids', *American Journal of Physics*, vol. 78, no. 3, pp. 229–235, Mar. 2010, doi: 10.1119/1.3256157.

[5] K. K. Liang, 'Efficient conversion from rotating matrix to rotation axis and angle by extending Rodrigues' formula'. arXiv, Oct. 09, 2018. doi: 10.48550/arXiv.1810.02999.

[6] 'UR10e Collaborative industrial robot - Payload up to 12.5 kg'. https://www.universal-robots.com/products/ur10-robot/ (accessed May 24, 2023).